

Identification of Phosphatidylinositol 3-Kinase δ (PI3K δ) Inhibitor: Pharmacophore-based Virtual Screening and Molecular Dynamics Simulation

Muhammad Arba^{1*}, Malindo Sufriadin¹, and Daryono Hadi Tjahjono²

¹Faculty of Pharmacy, Halu Oleo University, Jl. Kampus Hijau Bumi Tridharma, Anduonou, Kendari 93132, Southeast Sulawesi, Indonesia

²School of Pharmacy, Institut Teknologi Bandung, Jl. Ganesa No. 10, Bandung 40132, West Java, Indonesia

* **Corresponding author:**

email: muh.arba@uho.ac.id

Received: July 5, 2019

Accepted: July 27, 2019

DOI: 10.22146/ijc.47327

Abstract: Phosphatidylinositol 3-kinase δ (PI3K δ) is a validated drug target for the treatment of cancer. The present study aims to search for new inhibitors of PI3K δ by employing pharmacophore modelling using LigandScout Advanced 4.3 software. The three hydrogen bond acceptors and two hydrophobic features were proposed as a pharmacophore model using LASW1976 structure. The model was then validated using the Area Under Curve (AUC) of Receiver Operating Characteristic (ROC) and GH score. It was used to screen new molecules in the ZINC database, which resulted in 599 hits. All 599 hits were then docked into PI3K δ protein, and five best hits were submitted to 50 ns molecular dynamics simulations. Each hit complexed with PI3K δ underwent minor conformational changes as indicated by the values of Root Mean Square Deviation (RMSD) and Root Mean Square Fluctuation (RMSF). Furthermore, prediction of the binding free energy using Molecular Mechanics-Poisson Boltzmann Surface Area (MM-PBSA) method showed that five hits, i.e., Lig25/ZINC253496376, Lig682/ZINC98047241, Lig449/ZINC85878047, Lig554/ZINC253389510, and Lig199/ZINC12638303, had lower binding energy compared to LASW1976. This result indicated their potentials as new inhibitors of PI3K δ .

Keywords: PI3K; molecular docking; pharmacophore modeling; molecular dynamics simulation

■ INTRODUCTION

The phosphoinositide 3-kinases (PI3Ks) are a family of key enzymes that regulate numerous intracellular signal transduction pathways. The PI3K family is subdivided into three classes, i.e., Class I, Class II, and Class III. The Class-I PI3K family catalyzes the phosphorylation of phosphatidylinositol (4,5)-bisphosphate (PIP₂) to produce phosphatidyl-inositol(3,4,5)-trisphosphate (PIP₃) [1-2]. PIP₃ is a membrane-bound second messenger that activates downstream signaling pathways and crucial for cellular processes, such as proliferation, metabolism, and survival [3-4]. Class I, which bears regulatory and catalytic subunits, is subdivided into Class IA and Class IB. Class IA comprises of PI3K α , PI3K β , and PI3K δ , while Class IB includes PI3K γ [5].

Class-IA PI3K is activated by protein tyrosine kinase-coupled receptors, while Class IB is activated downstream by G-protein-coupled receptors. While PI3K α and PI3K β are ubiquitously expressed in all tissues, both PI3K δ and PI3K γ are predominantly found in hematopoietic cells, such as myeloid cells, B cells, and T cells [1,6]. The confined expression profile of PI3K δ suggests that its selective inhibition may be an interesting approach for the treatment of immune cell-related diseases, such as rheumatoid arthritis (RA), asthma, and hematological malignancies [5].

Idelalisib is the first inhibitor of PI3K δ , which is approved by Food and Drug Administration (FDA) to treat relapsed follicular B-cell non-Hodgkin's lymphoma (FL) and relapsed chronic lymphocytic leukemia (CLL) [7].

Another PI3K inhibitor, Copanlisib, has been recently approved for the treatment of follicular lymphoma [8-10]. Despite those facts, the finding of a new inhibitor of PI3K δ is urgently needed due to the side effects of the two agents, such as hepatic toxicity, diarrhea, colitis, and intestinal perforation [11]. However, the design of PI3K δ isoform has not been straightforward due to the similar ATP binding pockets between the isoforms. With the increasingly important role of computational drug design [12-13], the present study combines structure-based pharmacophore modeling with molecular docking to identify a potent inhibitor of PI3K δ . Furthermore, the combined molecular dynamics simulation and the molecular mechanics-Poisson Boltzmann Surface Area (MM-PBSA) methods were applied to explore the conformational change of ligand-receptor complex and to predict the binding affinity of the ligand to PI3K δ .

■ Computational Methods

Pharmacophore Modeling and Database Screening

The pharmacophore model was built by employing LigandScout Advanced 4.3 software [14] based on the 3D structure of PI3K δ -LASW1976 complex, which was retrieved from the Protein Data Bank (www.rcsb.org) with the PDB ID 6G6W [11]. The model was then validated by performing screening against 27 actives taken from BindingDB [15] and 1455 decoys retrieved from the Directory of Useful Decoys-Enhanced (DUD-E) [16].

Furthermore, Pharmit web server (<http://pharmit.csb.pitt.edu/>) [17] was used to screen hit molecules against the ZINC database using the validated pharmacophore [18]. The radius of each hydrogen bond donor/acceptor and hydrophobic features was 0.5 Å and 1 Å, respectively.

Molecular Docking and Molecular Dynamics Studies

Each hit molecule was docked into the active site of PI3K δ using iDock software [19]. The PI3K δ structure in complex with LASW1976 was retrieved from the Protein Data Bank (PDB ID: 6G6W) [11]. The receptor was prepared by using AutoDockTools 1.5.6., including adding polar hydrogen and assigning Kollman charges. The grid box for docking was set to the center of LASW1976

coordinates with a size of 22.5 × 22.5 × 22.5 Å in XYZ dimensions. The LASW1976 was redocked into PI3K δ to validate the docking protocol. Analysis and visualization of docked molecules were performed by using Discovery Studio Visualizer 2016. Five top molecules having the best binding affinities with good interaction were subjected to molecular dynamics simulation.

Molecular dynamics (MD) simulation was used to study the conformational changes in the interaction of ligands with PI3K δ . Five best docked ligands and native inhibitor (LASW1976), each complexed with PI3K δ , were chosen for MD simulation employing AMBER16 package [20-21]. Leap module of AMBER16 was used to prepare each ligand-protein complex. The ff14SB force field [22] was used to process protein, while GAFF force field [23] and AM1-BCC [24] were used to treat ligands. Each complex was immersed in a truncated octahedron TIP3P water box with a 10 Å radius. Counterions were added to the neutralized complex.

Each prepared complex underwent minimization using the sander program of AMBER16. The minimization was performed by 500 cycles of steepest descents and 5500 cycles of conjugate gradients methods in three steps: i) the protein was restrained with a force constant of 500 kcal mol⁻¹ Å⁻²; ii) the backbone atoms of protein were restrained with a force constant of 500 kcal mol⁻¹ Å⁻²; iii) minimization without restraint.

Furthermore, each system was gradually heated from 0 to 100, 100 to 200, and 200 to 300 K, respectively, for every 50 ps with a time step of 0.0005 ps and backbone atoms of protein were restrained with a force constant 5 kcal mol⁻¹ Å⁻². The system was then equilibrated at 300 K in three steps over a period of 200 ps. First and second equilibrations were performed for every 50 ps with force constants of 5 and 3 kcal mol⁻¹ Å⁻². Final 100 ps equilibration was conducted without restraint. A full production step was performed for 50 ns in NPT ensemble without any restraint employing pmemd.cuda module of AMBER16.

All bonds involving hydrogen atoms were constrained using SHAKE algorithm [25] with 2 fs integration time step. The particle-mesh Ewald

algorithm method was used to treat long-range electrostatics interactions [26] of a periodic box with a non-bonding cutoff distance of 9.0 Å. The Langevin thermostat was used to control Langevin thermostat with a collision rate of 1.0 ps⁻¹. The coordinate files were saved every 1 ps. Analyses were performed with the CPPTRAJ module of AMBER16 [27], while visualization was conducted using the Visual Molecular Dynamics software [28].

Binding Free Energy Calculation

The binding affinity of ligands to PI3Kδ was assessed through the binding free energy calculation using the Molecular Mechanics-Poisson Boltzmann solvent accessible surface area (MM-PBSA) method [29-30] of AMBER16 [31]. Trajectories with two hundred snapshots were taken from 30–50 ns MD simulation. The binding free energy (ΔG_{bind}) is calculated using the following equations:

$$\Delta G_{\text{bind}} = G_{\text{complex}} - G_{\text{rec}} - G_{\text{ligand}} \quad (1)$$

$$\Delta G_{\text{bind}} = \Delta E_{\text{MM}} + \Delta G_{\text{sol}} - T\Delta S \quad (2)$$

$$\Delta E_{\text{MM}} = \Delta E_{\text{bond}} + \Delta E_{\text{angle}} + \Delta E_{\text{torsion}} + \Delta E_{\text{vdw}} + \Delta E_{\text{EEL}} \quad (3)$$

$$\Delta G_{\text{sol}} = \Delta G_{\text{PB}} + \Delta G_{\text{SA}} \quad (4)$$

where G_{complex} , G_{rec} , and G_{lig} refer to the free energy of the complex, receptor, and ligand, respectively. The ΔG_{bind} consists of the binding energy in the vacuum/gas phase (ΔE_{MM}), the solvation free energy (ΔG_{sol}), and the conformational entropy change upon ligand binding at temperature T ($T\Delta S$). The ΔE_{MM} is the sum of bond energy (ΔE_{bond}), the angle energy (ΔE_{angle}), the torsion energy ($\Delta E_{\text{torsion}}$), the van der Waals energy (ΔE_{vdw}), and the electrostatic energy (ΔE_{EEL}). Meanwhile, ΔG_{sol} includes polar contribution to solvation free energy (ΔG_{PB}) calculated by solving the Poisson-Boltzmann (PB) equation using a grid size of 0.5 Å, and the non-polar contribution (ΔG_{SA}), which was calculated using the solvent accessible surface area (SASA) with the solvent-probe radius set to 1.4 Å.

RESULTS AND DISCUSSION

The pharmacophore model development resulted in a hypothesis consisting of three hydrogen bond acceptors and two hydrophobic features. Fig. 1 shows the

pharmacophore model generated on LigandScout 4.3 Advanced software.

Validation of the model against 27 actives and 1455 decoys resulted in Area Under Curve (AUC) of Receiver Operating Characteristic (ROC) of 0.67. The calculation of Goodness of Hit Score (GH-score) gave a result of 0.64. Both parameters indicated that the pharmacophore model was able to differentiate the actives from the decoy molecules. Fig. 2 displays the Area Under Curve (AUC) of Receiver Operating Characteristic (ROC) curve.

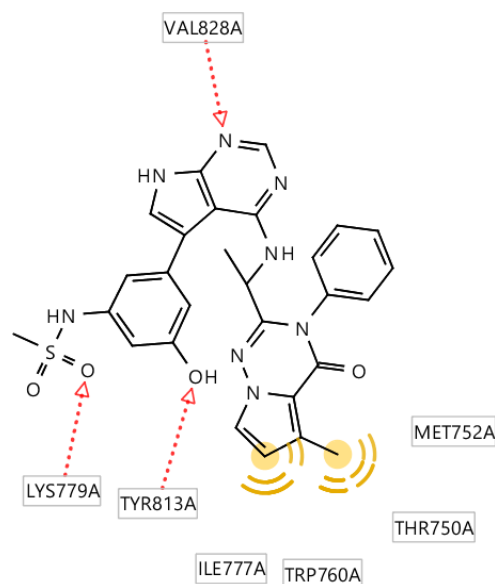


Fig 1. 3D pharmacophore model consisting of three hydrogen bond acceptors (red dotted lines) and two hydrophobic (yellow sphere) features

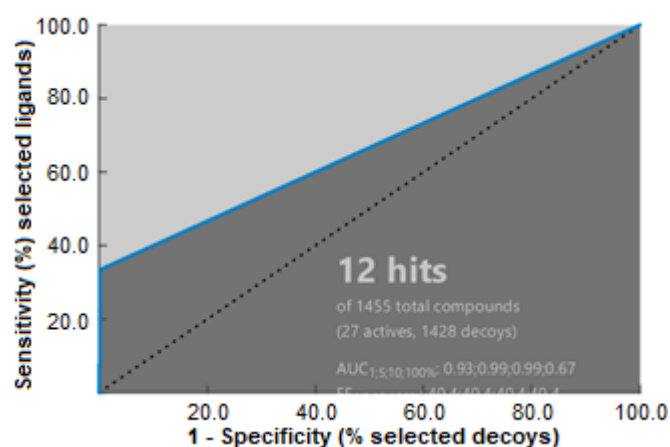


Fig 2. The Area Under Curve (AUC) of Receiver Operating Characteristic (ROC) curve

Furthermore, screening for hit molecules against the ZINC database by using the built pharmacophore model in Pharmit (<http://pharmit.csb.pitt.edu/>) retrieved 599 hit molecules. All 599 hits were then docked into PI3K δ using iDock, which gave conformations and binding energies ranging from -3.26 to -10.68 kcal/mol. Meanwhile, redocking of LASW1976 produced a similar conformation to the X-ray pose (root mean square deviation, RMSD=1.04 Å) and binding energy of -10.99 kcal/mol, which indicated that the docking protocol was valid [32]. All hydrogen bonds (Hbonds) of X-ray experiment were reproduced in a docked pose such as those with Lys779, Asp787, Tyr813, and Val828. Additional Hbond interaction of docked conformation was found between LASW1976 and Asp911. Fig. 3 shows the superimposed LASW1976 conformations of both experimental and docked experiments.

Based on the binding energies and conformations, five best docked hit molecules were selected. They were Lig25/ZINC253496376 ($E=-10.68$ kcal/mol), Lig682/ZINC98047241 ($E=-10.68$ kcal/mol), Lig449/ZINC85878047 ($E=-10.54$ kcal/mol), Lig554/ZINC253389510 ($E=-10.29$ kcal/mol), and Lig199/ZINC12638303 ($E=-10.28$ kcal/mol).

Fig. 4 shows the chemical structures of the five best docked hit molecules.

In the meantime, the binding of hit molecules occurred through several Hbond and hydrophobic interactions. Lig25/ZINC253496376 formed two Hbond interactions with Lys779 through oxygen atoms of

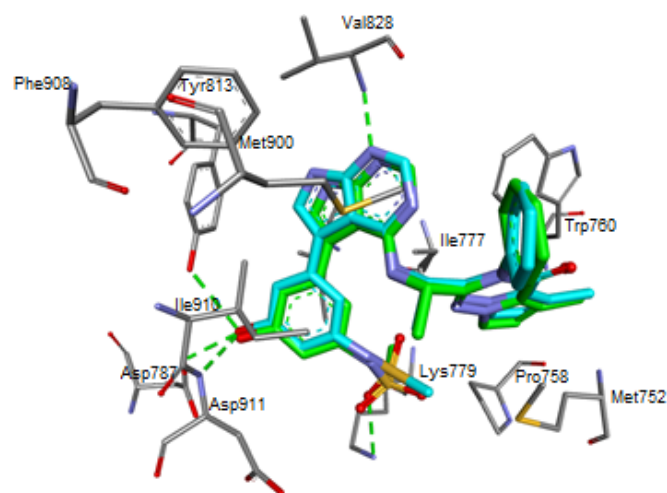


Fig 3. The superimposed LASW1976 conformations of both experimental (green) and docked (blue) experiments. The hydrogen bonds are represented in green colored dashed lines

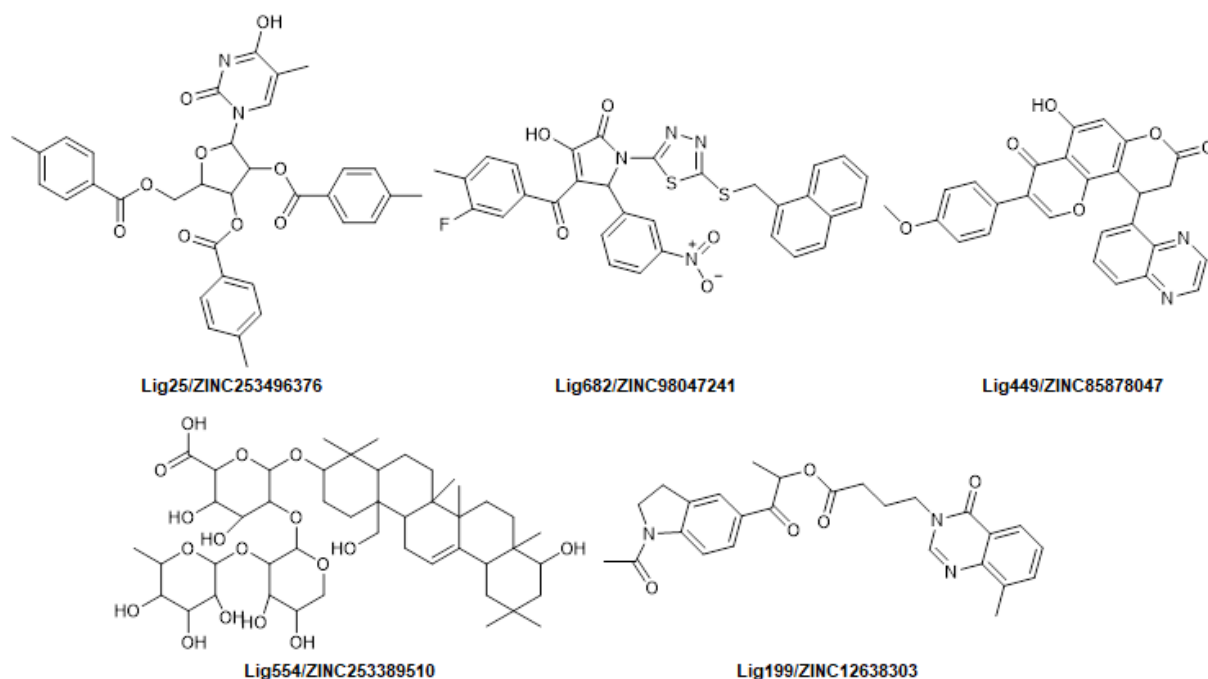


Fig 4. The chemical structures of the five best docked hit molecules

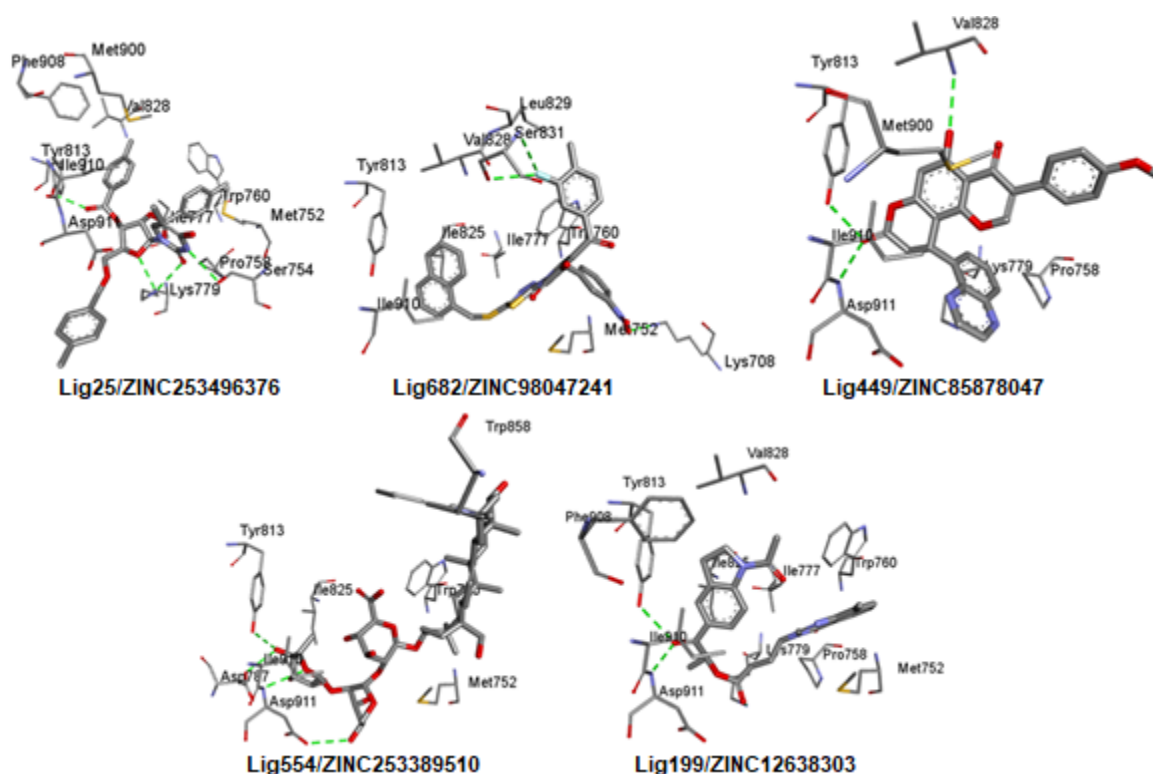


Fig 5. The binding modes of each hit molecules, i.e., Lig25/ZINC253496376, Lig682/ZINC98047241, Lig449/ZINC 85878047, Lig554/ZINC253389510, Lig199/ZINC12638303, into the active site of PI3K δ . The hydrogen bonds are represented in green colored dashed lines

pyrimidine and oxolane groups. The nitrogen atom of the pyrimidine group also formed Hbond with Ser754, while Tyr813 formed Hbond with the oxygen atom of the carbonyl group. Lig682/ZINC98047241 formed Hbond interaction through an oxygen atom of phenylnitroso oxidanol group with Lys708 and two Hbond interactions between the fluorine atom of the ligand with Ser831 were also established. Amino acid residues Tyr813 along with Asp911 also formed Hbonds with Lig449/ZINC85878047 through an oxygen atom of pyran group, in addition to Val828 which formed Hbond interaction with the oxygen atom of the phenyl group. Tyr813 and Asp911 were both found to establish two Hbond interactions in the binding of Lig554/ZINC 253389510, in addition to the one with Asp787. The binding of Lig199/ZINC12638303 was also corroborated with Hbond interactions between oxygen atoms of two carbonyl groups and Tyr813 and Asp911, as well as Lys779. Fig. 5 displays the binding modes of each hit molecules into the active site of PI3K δ .

Molecular Dynamics Simulations

Five best docked hit molecules to PI3K δ were subjected to MD simulation for 50 ns to assess their conformational changes in a physiological condition. The values of root mean square deviation (RMSD), which is considered as a parameter for the stability of complex during dynamics runs, were calculated. Fig. 6 shows the RMSD values of heavy atoms (Ca, C, N, O) of the protein. There was a sudden increase in the early stage of simulation (0–20 ns) for all ligands, but it soon became stable throughout the simulation. The Lig682/ZINC98047241 (pink) and Lig554/ZINC253389510 (purple) displayed lower RMSD values than the cognate ligand (LASW1976, red) did, indicating their more stable conformational changes. On the other hand, although Lig25/ZINC253496376 (green), Lig449/ZINC 85878047 (blue), and Lig199/ZINC12638303 (cyan) showed more fluctuated changes than LASW1976 (red), their movements tended to be stable in the rest simulation.

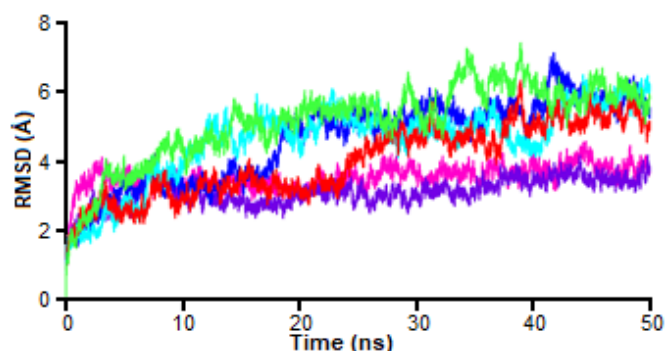


Fig 6. RMSD value of protein heavy atom of each ligand-PI3K δ complex during 50 ns MD calculated for LASW1976 (red), Lig25/ZINC253496376 (green), Lig682/ZINC98047241 (pink), Lig449/ZINC85878047 (blue), Lig554/ZINC253389510 (purple), and Lig199/ZINC12638303 (cyan)

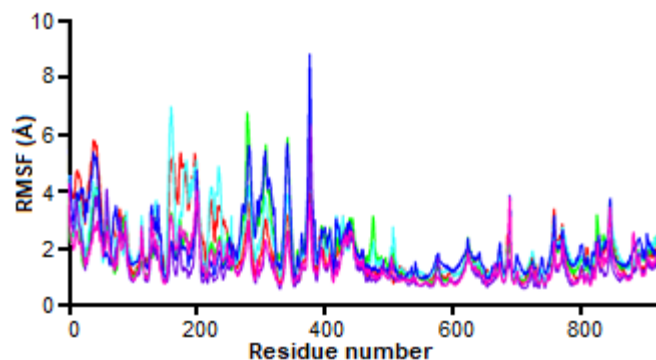


Fig 7. RMSF change during 50 ns MD simulation for LASW1976 (red), Lig25/ZINC253496376 (green), Lig682/ZINC98047241 (pink), Lig449/ZINC85878047 (blue), Lig554/ZINC253389510 (purple), and Lig199/ZINC12638303 (cyan)

In addition to the RMSD plot, atomic fluctuation along amino acid residues of the PI3K δ during dynamics runs were monitored in root mean square fluctuation (RMSF) plot (Fig. 7). It shows that amino acid residues fluctuated in a similar pattern in all regions of the protein, indicating the similar binding modes of hit molecules. Higher values of RMSF were found at peaks of Tyr39 (Tyr55), Asp279 (Asp336), Val308 (Val365), Glu376 (Glu448), and Ser688 (Ser770), which were attributable to the loop regions. In addition, Pro160 (Pro186) and Glu342 (Glu399) were also dominant and corresponded to the ends of beta-helix. On the other hand, amino acid residues involved in the Hbond interactions over all ligands, such as Lys708, Ser754, Lys779, Asp787, Tyr813, Val828, Ser831, and Asp911, appeared to be more rigid, indicating that ligand binding induced stability over the protein fluctuation.

Monitoring the conformation of each hit after 50-ns MD simulation revealed several changes were noted in the poses of hit molecules. Hit molecule Lig25/ZINC253496376 formed conventional Hbond interaction with Asn754, C—H \cdots O hydrogen bond interaction with Ser672, as well as pi-alkyl interactions with Tyr731, Met670, and Ile815. Lig682/ZINC98047241 formed conventional Hbond interactions with Lys626, Thr751, Asn754, and Asp750, as well as C—H \cdots O hydrogen bond interaction with Met670. In addition, pi-sulfur contact occurred with Met670. Pi-alkyl interaction was observed

with Met680, Trp678, Met805, Ile695, Ile743, and Ile815, while pi-pi interaction occurred with Trp678. Pi-alkyl interactions were also noted between Lig449/ZINC85878047 with Ile815, Met670, Val745, and Met805, while pi-pi interaction was observed with Trp678. Meanwhile, Lig554/ZINC253389510 established conventional Hbond interactions with Lys697, Val746, and Glu744, as well as pi alkyl interactions with Trp678 and Tyr731. Conventional Hbond interaction was also formed between Lig199/ZINC12638303 and Asp816. While pi-alkyl interactions were noted between Lig199/ZINC12638303 and Trp678, Met670, Ile695, and Ile815. The binding of Lig199/ZINC12638303 was also corroborated by pi-pi interaction with Trp678. Fig. 8 showed each mode of interaction of each hit molecule after 50 ns MD simulation.

Monitoring of the Hbonds during dynamics run showed that the Hbonds interactions showed fair occupancies during molecular dynamics simulation. For example, the Hbonds of Lig199/ZINC12638303 with Asp911 and Lys779 showed fair occupancies of 29.37% and 17.73%, respectively. Meanwhile, the Hbond with Tyr813 showed very low occupancy which was only 0.56%. In the Lig554/ZINC253389510 binding, several Hbonds between ligand atoms and Asp911 were found with occupancies ranging from 1.03% to 15.4%. Whereas, Hbonds between Lig554/ZINC253389510 and Val828 had 4.10% and 11.6% occupancies. The Lig449/ZINC85878047

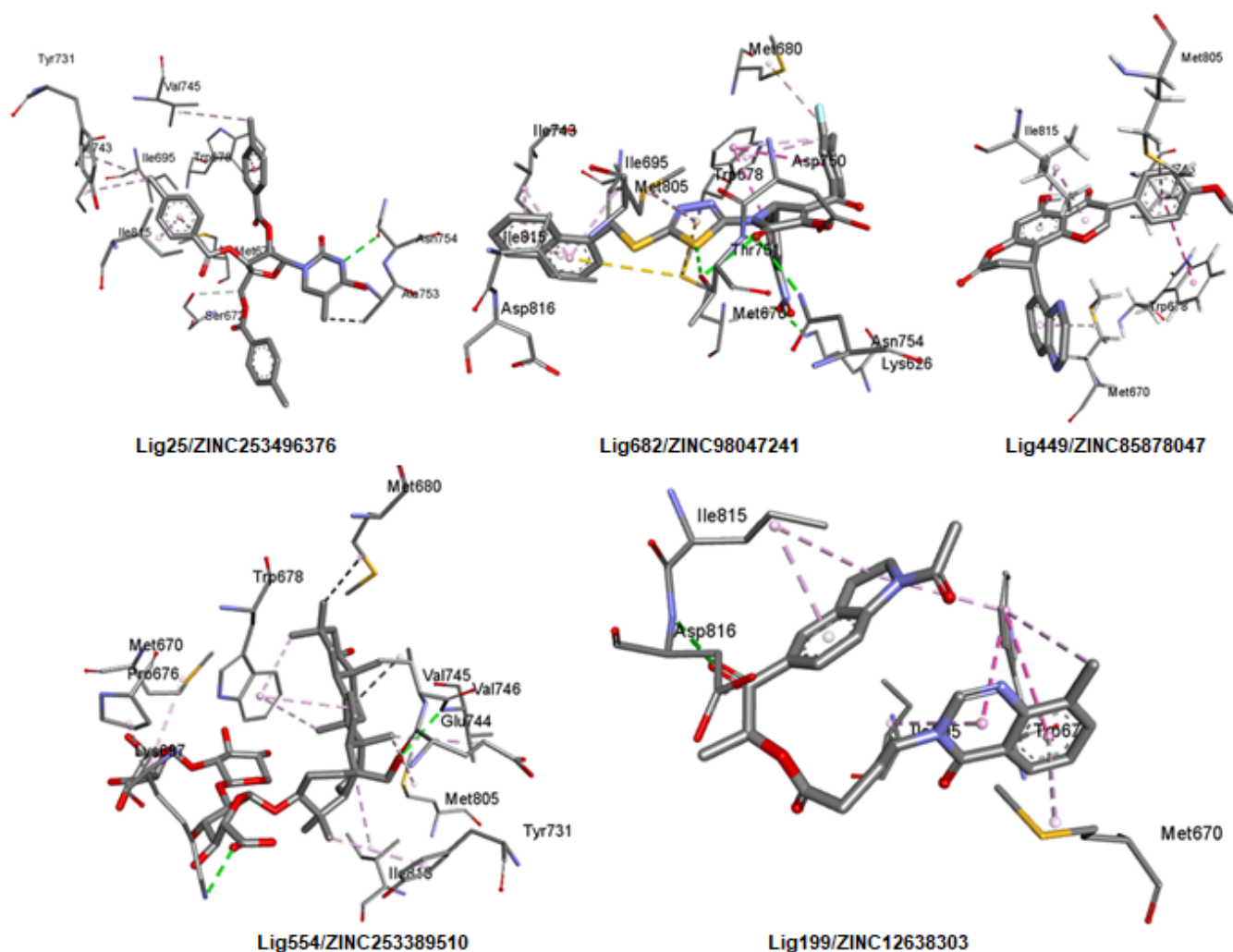


Fig 8. Conformation of each hit molecule after 50 ns MD simulation. The hydrogen bond, C—H···O hydrogen bond, pi-alkyl, pi-pi, pi-sulfur interactions are represented in green, pale blue, pink, magenta, and yellow colored dashed lines, respectively

showed that the Hbonds with Ser754, Asp911, and Tyr813 had the occupancies of 12.56, 3.98, and 0.94%, respectively. While Lig25/ZINC253496376 had several Hbonds with Lys779 with the occupancies of 4.29 to 6.08%, while that with Ser754 showed very low occupancies of 4.1%.

On the other hand, several new Hbonds were found during MD simulation. The new Hbonds were, for example, Hbonds between Lig682/ZINC98047241 and Asp832 and Thr833 with occupancies of 96.26 and 52.23%, respectively. The Hbond with Asp832 was also found in the binding of Lig554/ZINC253389510 with occupancy of 15.99%. In addition, Hbond with Asn836 was found

doubly in the binding of Lig25/ZINC253496376 with occupancies of 18.17 and 12.58%. Meanwhile, that with Lig449/ZINC85878047 showed 3.61% occupancy. On the other hand, Hbond with Glu826 was found with 17.43% occupancy in the binding of Lig554/ZINC253389510. Table S1 shows the Hbond occupancies during the 50 ns simulation.

Free Binding Energy Calculations

The five best docked hit molecules were subjected to free binding energy calculation using the MM-PBSA method. The MM-PBSA method is widely considered to be more accurate compared to the docking scoring. Table 1

Table 1. The binding free energy and their individual energy contributions

Ligand	ΔE_{ELE} (kcal/mol)	ΔE_{VDW} (kcal/mol)	ΔE_{PBCAL} (kcal/mol)	ΔE_{PBSUR} (kcal/mol)	ΔE_{PBTOT} (kcal/mol)
LASW1976	-15.54±6.17	-49.03±3.84	53.15±7.99	-4.84±0.18	-16.27±4.54
Lig25/ZINC253496376	-29.24±13.14	-44.58±5.50	54.01±12.75	-5.24±0.41	-25.05±4.96
Lig199/ZINC12638303	-24.79±4.33	-56.99±2.99	53.38±4.54	-5.25±0.11	-33.64±3.69
Lig449/ZINC85878047	2.96±7.43	-38.78±3.83	23.73±6.95	-4.49±0.21	-16.58±5.96
Lig554/ZINC253389510	-32.85±21.38	-52.19±6.04	58.56±20.15	-5.63±0.41	-38.27±8.90
Lig682/ZINC98047241	-32.96±4.96	-45.14±4.60	53.67±5.41	-5.37±0.22	-29.80±3.97

displays the binding free energy and their individual energy contributions. The hit molecule Lig554/ZINC 253389510 had the lowest predicted binding free energy ($\Delta E_{PBTOT} = -38.27 \pm 8.90$ kcal/mol), about 2 times more negative than that of LASW1976 ($\Delta E_{PBTOT} = -16.27 \pm 4.54$ kcal/mol). The binding energy value for a good inhibitor was considered in the range of -9 to -12 kcal/mol, however, the much lower binding energy value obtained in the present study corresponded to the excluded entropy term in the calculation [30]. Furthermore, the hit molecule Lig199/ZINC12638303 scored the second best binding free energy ($\Delta E_{PBTOT} = -33.64 \pm 3.69$ kcal/mol), followed by the molecule hits Lig682/ZINC98047241 ($\Delta E_{PBTOT} = -29.80 \pm 3.97$ kcal/mol), Lig25/ZINC253496376 ($\Delta E_{PBTOT} = -25.05 \pm 4.96$ kcal/mol), and Lig449/ZINC85878047 ($\Delta E_{PBTOT} = -16.58 \pm 5.96$ kcal/mol). The major favorable contributions to ligand binding at PI3K δ were originated from electrostatic (ΔE_{ELE}), van der Waals (ΔE_{VDW}), and non-polar solvation energy (ΔE_{PBSUR}), except for Lig449/ZINC85878047 which had positive electrostatic energy. Overall, all hit molecules displayed stronger affinities than LASW1976 did.

CONCLUSION

Structure-based pharmacophore modelling was performed based on PI3K δ -LASW1976 interaction. The pharmacophore model was built and validated based on the Area Under Curve of Receiver Operating Characteristic and GH-score. It was then used to identify hit molecules in the ZINC database. Five hundred and ninety-nine hit molecules were retrieved and then docked to the active site of PI3K δ to reveal their binding modes. Hit molecules maintained their interactions with the PI3K δ through important Hbond and hydrophobic interactions. Five

best hits were selected and subjected to MD simulation, which showed good stability during 50 ns. Prediction of binding free energy using the MM-PBSA method showed that the five hit molecules displayed stronger affinities than LASW1976 did. The van der Waals, electrostatic, and nonpolar contribution to the solvation energy interactions were favorable for most hit molecules. The present work suggests five hit molecules that might serve as potential inhibitors of PI3K δ .

ACKNOWLEDGMENTS

The present research was partly funded by the Ministry of Research and the Higher Education Republic of Indonesia through Hibah Penelitian Dasar 2019.

REFERENCES

- [1] Ameriks, M.K., and Venable, J.D., 2009, Small molecule inhibitors of phosphoinositide 3-kinase (PI3K) delta and gamma, *Curr. Top. Med. Chem.*, 9 (8), 738–753.
- [2] Hoegenauer, K., Soldermann, N., Hebach, C., Hollingworth, G.J., Lewis, I., von Matt, A., Smith, A.B., Wolf, R.M., Wilcken, R., Haasen, D., Burkhart, C., and Zécric, F., 2016, Discovery of novel pyrrolidineoxy-substituted heteroaromatics as potent and selective PI3K delta inhibitors with improved physicochemical properties, *Bioorg. Med. Chem. Lett.*, 26 (23), 5657–5662.
- [3] Vanhaesebroeck, B., Stephens, L., and Hawkins, P., 2012, PI3K signalling: The path to discovery and understanding, *Nat. Rev. Mol. Cell Biol.*, 13 (3), 195–203.
- [4] Ma, C.C., Zhang, C.M., Tang, L.Q., and Liu, Z.P., 2018, Discovery of novel quinazolinone derivatives

- as high potent and selective PI3K δ and PI3K δ / γ inhibitors, *Eur. J. Med. Chem.*, 151, 9–17.
- [5] Hoegenauer, K., Soldermann, N., Stauffer, F., Furet, P., Graveleau, N., Smith, A.B., Hebach, C., Hollingworth, G.J., Lewis, I., Gutmann, S., Rummel, G., Knapp, M., Wolf, R.M., Blanz, J., Feifel, R., Burkhart, C., and Zécéri, F., 2016, Discovery and pharmacological characterization of novel quinazoline-based PI3K delta-selective inhibitors, *ACS Med. Chem. Lett.*, 7 (8), 762–767.
- [6] Rowan, W.C., Smith, J.L., Affleck, K., and Amour, A., 2012, Targeting phosphoinositide 3-kinase δ for allergic asthma, *Biochem. Soc. Trans.*, 40 (1), 240–245.
- [7] Nair, K.S., and Cheson, B., 2016, The role of idelalisib in the treatment of relapsed and refractory chronic lymphocytic leukemia, *Ther. Adv. Hematol.*, 7 (2), 69–84.
- [8] Göckeritz, E., Kerwien, S., Baumann, M., Wigger, M., Vondrey, V., Neumann, L., Landwehr, T., Wendtner, C.M., Klein, C., Liu, N., Hallek, M., Frenzel, L.P., and Krause, G., 2015, Efficacy of phosphatidylinositol-3 kinase inhibitors with diverse isoform selectivity profiles for inhibiting the survival of chronic lymphocytic leukemia cells, *Int. J. Cancer*, 137 (9), 2234–2242.
- [9] Bashash, D., Safaroghli-Azar, A., Dadashi, M., Safa, M., Momeny, M., and Ghaffari, S.H., 2017, Anti-tumor activity of PI3K- δ inhibitor in hematologic malignant cells: Shedding new light on resistance to Idelalisib, *Int. J. Biochem. Cell Biol.*, 85, 149–158.
- [10] Flinn, I.W., Patel, M., Oki, Y., Horwitz, S., Foss, F.F., Allen, K., Douglas, M., Stern, H., Sweeney, J., Kharidia, J., Kelly, P., Kelly, V.M., and Kahl, B., 2018, Duvelisib, an oral dual PI3K- δ , γ inhibitor, shows clinical activity in indolent non-Hodgkin lymphoma in a phase 1 study, *Am. J. Hematol.*, 93 (11), 1311–1317.
- [11] Erra, M., Taltavull, J., Bernal, F.J., Caturla, J.F., Carrascal, M., Pagès, L., Mir, M., Espinosa, S., Gràcia, J., Domínguez, M., Sabaté, M., Paris, S., Maldonado, M., Hernández, B., Bravo, M., Calama, E., Miralpeix, M., Lehner, M.D., and Calbet, M., 2018, Discovery of a novel inhaled PI3K δ inhibitor for the treatment of respiratory diseases, *J. Med. Chem.*, 61 (21), 9551–9567.
- [12] Arba, M., Nur-Hidayat, A., Surantaadmaja, S.I., and Tjahjono, D.H., 2018, Pharmacophore-based virtual screening for identifying β 5 subunit inhibitor of 20S proteasome, *Comput. Biol. Chem.*, 77, 64–71.
- [13] Arba, M., Yamin, Ihsan, S., and Tjahjono, D.H., 2018, Computational approach toward targeting the interaction of porphyrin derivatives with Bcl-2, *J. Appl. Pharm. Sci.*, 8 (12), 60–66.
- [14] Wolber, G., and Langer, T., 2005, LigandScout: 3-D pharmacophores derived from protein-bound ligands and their use as virtual screening filters, *J. Chem. Inf. Model.*, 45 (1), 160–169.
- [15] Gilson, M.K., Liu, T., Baitaluk, M., Nicola, G., Hwang, L., and Chong, J., 2016, BindingDB in 2015: A public database for medicinal chemistry, computational chemistry and systems pharmacology, *Nucleic Acids Res.*, 44 (D1), D1045–D1053.
- [16] Mysinger, M.M., Carchia, M., Irwin, J.J., and Shoichet, B.K., 2012, Directory of useful decoys, enhanced (DUD-E): Better ligands and decoys for better benchmarking, *J. Med. Chem.*, 55 (14), 6582–6594.
- [17] Sunseri, J., and Koes, D.R., 2016, Pharmit: interactive exploration of chemical space, *Nucleic Acids Res.*, 44 (W1), W442–W448.
- [18] Irwin, J.J., Sterling, T., Mysinger, M.M., Bolstad, E.S., and Coleman, R.G., 2012, ZINC: A free tool to discover chemistry for biology, *J. Chem. Inf. Model.*, 52 (7), 1757–1768.
- [19] Li, H., Leung, K.S., and Wong, M.H., 2012, Idock: A multithreaded virtual screening tool for flexible ligand docking, 2012 *IEEE Symposium on Computational Intelligence in Bioinformatics and Computational Biology (CIBCB)*, San Diego, California, USA, 9–12 May 2012, 77–84.
- [20] Case, D.A., Cheatham, T.E., Darden, T., Gohlke, H., Luo, R., Merz, K.M., Onufriev, A., Simmerling, C., Wang, B., and Woods, R.J., 2005, The Amber biomolecular simulation programs, *J. Comput. Chem.*, 26 (16), 1668–1688.

- [21] Salomon-Ferrer, R., Götz, A.W., Poole, D., Le Grand, S., and Walker, R.C., 2013, Routine microsecond molecular dynamics simulations with AMBER on GPUs. 2. Explicit solvent particle mesh Ewald, *J. Chem. Theory Comput.*, 9 (9), 3878–3888.
- [22] Maier, J.A., Martinez, C., Kasavajhala, K., Wickstrom, L., Hauser, K.E., and Simmerling, C., 2015, ff14SB: Improving the accuracy of protein side chain and backbone parameters from ff99SB, *J. Chem. Theory Comput.*, 11 (8), 3696–3713.
- [23] Wang, J., Wolf, R.M., Caldwell, J.W., Kollman, P.A., and Case, D.A., 2004, Development and testing of a general amber force field, *J. Comput. Chem.*, 25 (9), 1157–1174.
- [24] Jakalian, A., Jack, D.B., and Bayly, C.I., 2002, Fast, efficient generation of high-quality atomic charges. AM1-BCC model: II. Parameterization and validation, *J. Comput. Chem.*, 23 (16), 1623–1641.
- [25] Ryckaert, J.P., Ciccotti, G., and Berendsen, H.J.C., 1977, Numerical integration of the Cartesian equations of motion of a system with constraints: Molecular dynamics of *n*-alkanes, *J. Comput. Phys.*, 23 (3), 327–341.
- [26] Darden, T., York, D., and Pedersen, L., 1993, Particle mesh Ewald: An $N \cdot \log(N)$ method for Ewald sums in large systems, *J. Chem. Phys.*, 98 (12), 10089.
- [27] Roe, D.R., and Cheatham III, T.E., 2013, PTRAJ and CPPTRAJ: Software for processing and analysis of molecular dynamics trajectory data, *J. Chem. Theory Comput.*, 9 (7), 3084–3095.
- [28] Humphrey, W., Dalke, A., and Schulten, K., 1996, VMD: Visual molecular dynamics, *J. Mol. Graphics*, 14 (1), 33–38.
- [29] Kollman, P.A., Massova, I., Reyes, C., Kuhn, B., Huo, S., Chong, L., Lee, M., Lee, T., Duan, Y., Wang, W., Donini, O., Cieplak, P., Srinivasan, J., Case, D.A., and Cheatham, T.E., 2000, Calculating structures and free energies of complex molecules: Combining molecular mechanics and continuum models, *Acc. Chem. Res.*, 33 (12), 889–897.
- [30] Arba, M., Kartasasmita, R.E., and Tjahjono, D.H., 2016, Molecular docking and dynamics simulations on the interaction of cationic porphyrin-anthraquinone hybrids with DNA G-quadruplexes, *J. Biomol. Struct. Dyn.*, 34 (2), 427–438.
- [31] Miller, B.R., McGee, T.D., Swails, J.M., Homeyer, N., Gohlke, H., and Roitberg, A.E., 2012, MMPBSA.py: An efficient program for end-state free energy calculations, *J. Chem. Theory Comput.*, 8 (9), 3314–3321.
- [32] Morris, G.M., Goodsell, D.S., Halliday, R.S., Huey, R., Hart, W.E., Belew, R.K., and Olson, A.J., 1998, Automated docking using a Lamarckian genetic algorithm and an empirical binding free energy function, *J. Comput. Chem.*, 19 (14), 1639–1662.